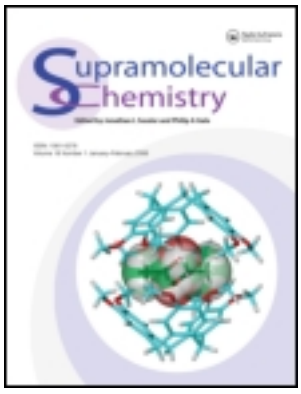

Supramolecular Chemistry
Publication details, including instructions for authors and subscription information:
http://www.tandfonline.com/loi/gsch20

STM studies on double- and triple-decker porphyrin and phthalocyanine complexes

Joe Otsuki [a]

[a] College of Science and Technology, Nihon University, 1-8-14 Kanda Surugadai, Chiyoda-ku, Tokyo, 101-8308, Japan

Available online: 13 Apr 2011

To cite this article: Joe Otsuki (2011): STM studies on double- and triple-decker porphyrin and phthalocyanine complexes, Supramolecular Chemistry, 23:03-04, 169-182

To link to this article: http://dx.doi.org/10.1080/10610278.2010.515028

Supramolecular Chemistry
Vol. 23, Nos. 3–4, March–April 2011, 169–182

STM studies on double- and triple-decker porphyrin and phthalocyanine complexes

Joe Otsuki*

College of Science and Technology, Nihon University, 1-8-14 Kanda Surugadai, Chiyoda-ku, Tokyo 101-8308, Japan

(*Received 5 June 2010; final version received 27 July 2010*)

Properly designed double- and triple-decker porphyrin and/or phthalocyanine complexes assemble themselves into ordered higher-order structures on substrate surfaces. One of the macrocyclic ligands adsorbs on the surface almost always in a face-on fashion on highly oriented pyrolytic graphite and Au(111) surfaces as revealed by means of scanning tunnelling microscopy. For example, well-ordered oriented monolayer assemblies of single-molecule magnets were fabricated. In some cases, the vertical orientation, that is, which ligand adsorbs on the surface, can be controlled by applied potentials. The rotational libration of the top ligand with respect to the adsorbed bottom ligand and hence to the surface has been visualised for a double-decker porphyrin with a molecular beacon. The electronic, magnetic and dynamic properties of double- and triple-decker complexes bode well for the development of molecular devices.

Keywords: double-decker complexes; molecular devices; phthalocyanines; porphyrins; scanning tunnelling microscopy

1. Introduction

Supramolecular chemistry on surfaces is an important and challenging field for the development of molecule-based devices, especially in view of connecting molecules to the macroscopic world. We have to know how molecules assemble themselves into higher-order structures to obtain desirable molecular organisations in a predictable manner. Molecules that are to be used as components for molecular devices should have a built-in program for higher organisation in their molecular structures. The programs will be decoded not only through intermolecular interactions, as in the case of three-dimensional assemblies (*1–3*), but also via molecule–substrate interactions in the case of assemblies on surfaces.

Scanning tunnelling microscopy (STM) provides chemists a unique opportunity to observe individual molecules in real space, once the molecules are immobilised on a surface (*4–16*). Thus, various molecules and molecular assemblies have been analysed by means of STM on various substrates. Among many molecules that have been analysed, tetrapyrrole compounds, i.e. porphyrins and phthalocyanines, constitute an especially interesting class of compounds for studies at the single-molecule level due to their rich electronic and photonic, to name a few, properties (*16*, *17*).

In this mini-review, I focus on surface assemblies of double- and triple-decker sandwich complexes among the tetrapyrrole families. Double-decker sandwich complexes consist of a rare-earth metal ion located between two macrocyclic tetrapyrrole ligands (porphyrins, phthalocyanines and/or naphthalocyanines) (Figure 1) (*18–25*). Structurally, the macrocyclic tetrapyrrole ligands are rotated with respect to each other by 45° around their normal axis so that the metal ion is eight-fold coordinated with the nitrogen atoms. Double-decker complexes are receiving much attention due to their rich functional properties, including semi-conductivity, electrochromicity and nonlinear optical properties. Owing to these properties, applications in colour display devices, Schottky junctions, *p–n* junctions, bipolar transistors, field-effect transistors, nonlinear optical materials and chemical sensors are envisaged. Double-decker complexes substituted with long hydrocarbon chains behave as liquid crystal materials as reported by Piechocki and co-workers in 1985 (*26*). Double-decker complexes also exhibit interesting dynamic behaviour such as rotational libration of the macrocyclic ligands with respect to each other (*18*, *20*, *27–35*). The rotational rates can be controlled by external stimuli, such as pH changes, redox reactions and addition of guest ions and molecules. Thus, the development of molecular rotors can be envisaged based on double-decker complexes. In addition to the rotational motion, trampoline-like movement of the ligands has also been suggested (*36*). More recently, Ishikawa and co-workers (*37*) have discovered that terbium phthalocyanine double-decker complexes function as single-molecule magnets. Triple-decker complexes have a motif of ligand–metal–ligand–metal–ligand, in which the three ligands, as well as the two metals, may or may not be identical.

This review is divided into two parts. The first part (Section 2) deals with static, structural aspects of self-assembled monolayer organisations. Section 2 is further

*Email: otsuki@chem.cst.nihon-u.ac.jp

ISSN 1061-0278 print/ISSN 1029-0478 online

DOI: 10.1080/10610278.2010.515028
http://www.informaworld.com

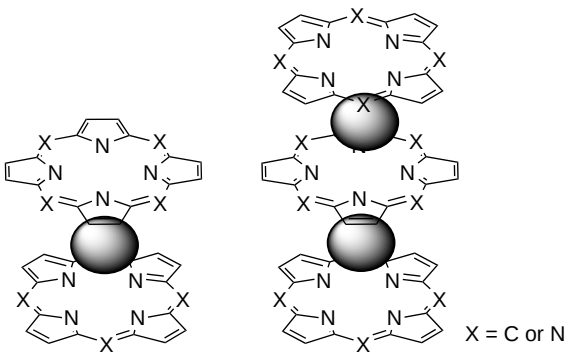

Figure 1. Cores of double- and triple-decker porphyrin/phthalocyanine complexes.

divided into two parts according to the substrate used, i.e. highly oriented pyrolytic graphite (HOPG) and Au(111). The former is further classified into single-component assemblies and multi-component assemblies. Apart from this classification, terbium phthalocyanine complexes are described in a separate subsection, because their properties as single-molecule magnets seem to deserve special attention. The second part (Section 3) deals with dynamic aspects of the assemblies. One is flip-flop motions of the triple-decker complexes as whole molecules and the other is rotational libration of the macrocyclic ligands within a double-decker complex. Finally, a brief conclusion is presented on the prospects of the double- and triple-decker complexes for the development of molecular devices. Double- and triple-decker complexes that have been observed with STM are listed in Table 1 and chemical structures of phthalocyanine and naphthalocyanine units and porphyrin units are displayed in Figures 2 and 3, respectively.

2. Self-assembly on surfaces

Two-dimensional (2D) assemblies of double-decker porphyrin/phthalocyanine complexes have been prepared mostly on HOPG or Au(111). There are only a few reports that a double-decker complex ([Ti(Pc)$_2$]) was deposited on other substrates: GaAs (*38*) and Cu(111) (*39*).

Table 1. STM studies on double-and triple-decker complexes.

Compounds	Substrate	Conditions	Ref.
[Ce(C_8OPc)$_2$]	HOPG	1-Phenyloctane	(*44*)
[Ce(C_8OPc)$_2$]	Au(111)	0.1 M $HClO_4$	(*52*)
[Ce(Pc)(C_8OPc)]	HOPG	1-Phenyloctane	(*44*)
[Ce(TPP)(C_8OPc)]	HOPG	1-Phenyloctane	(*44*)
[Ce(C_{12}OPc)$_2$]	HOPG	1-Phenyloctane	(*44*)
[Ce(Pc)(C_{22}OPP)]	HOPG	1-Phenyloctane	(*51*)
[Ce(C_{22}OPP)$_2$]	HOPG	1-Phenyloctane	(*51*)
[Ce(BPEPP)(C_{22}OPP)]	HOPG	1-Phenyloctane	(*51*)
[Ce(FcTPP)(C_{22}OPP)]	HOPG	1-Phenyloctane	(*62*)
[Ce_2(DBTP)$_3$]	Au(111)	UHV, 80 K	(*54*)
[Dy(Pc)$_2$]	Au(111)	UHV, 4 K	(*58*)
[(Pc)Dy(C_8OPc)Dy(Pc)]	HOPG	1-Phenyloctane	(*59*)
[Er(C_{12}OPc)$_2$]	HOPG	1-Phenyloctane	(*49*)
[Er(C_{12}OPc)$_2$]	HOPG	1,2,4-Trichlorobenzene	(*48*)
[Eu(CrPc)$_2$]	HOPG	1-Phenyloctane	(*59*)
[(TPP)Eu(CrPc)Eu(CrPc)]	Au(111)	0.05 M $HClO_4$	(*61*)
[LuH(Pc)$_2$]	HOPG	Solvent not described	(*40*)
[Lu(Pc)$_2$]	HOPG	LB membrane; air	(*41*)
[Lu(C_8OPc)$_2$]	HOPG	1-Phenyloctane	(*45*)
[Lu(Pc)(C_8OPc)]	HOPG	1-Phenyloctane	(*47*)
[Lu(Nc)(C_8OPc)]	HOPG	1-Phenyloctane	(*47*)
[Lu(iC_5OPc)(Nc)]	HOPG	1-Phenyloctane	(*50*)
[Lu(OEP)(Nc)]	HOPG	1-Phenyloctane	(*50*)
[Lu(TBPP)(Nc)]	HOPG	1-Phenyloctane	(*50*)
[(CrPc)Lu(CrPc)Lu(C_8OPc)]	HOPG	1-Phenyloctane	(*59*, *60*)
[Pr(C_8OPc)$_2$]	HOPG	1-Phenyloctane	(*46*)
[Tb(Pc)$_2$]	Au(111)	UHV, 4 K	(*58*)
[Tb(Pc)$_2$]	Cu(111)	UHV, 10 K	(*39*)
[Tb(C_4OPc)$_2$]	HOPG	Air	(*43*)
[Ti(Pc)$_2$]	HOPG	UHV	(*38*)
[Ti(Pc)$_2$]	GaAs(100)	UHV	(*38*)
[Y(Pc)$_2$]	Au(111)	UHV, 4.8 K	(*53*)
[Y(Pc)$_2$]	Au(111)	UHV, 4 K	(*58*)
[Y(C_8OPc)$_2$]	Au(111)	0.1 M $HClO_4$	(*52*)

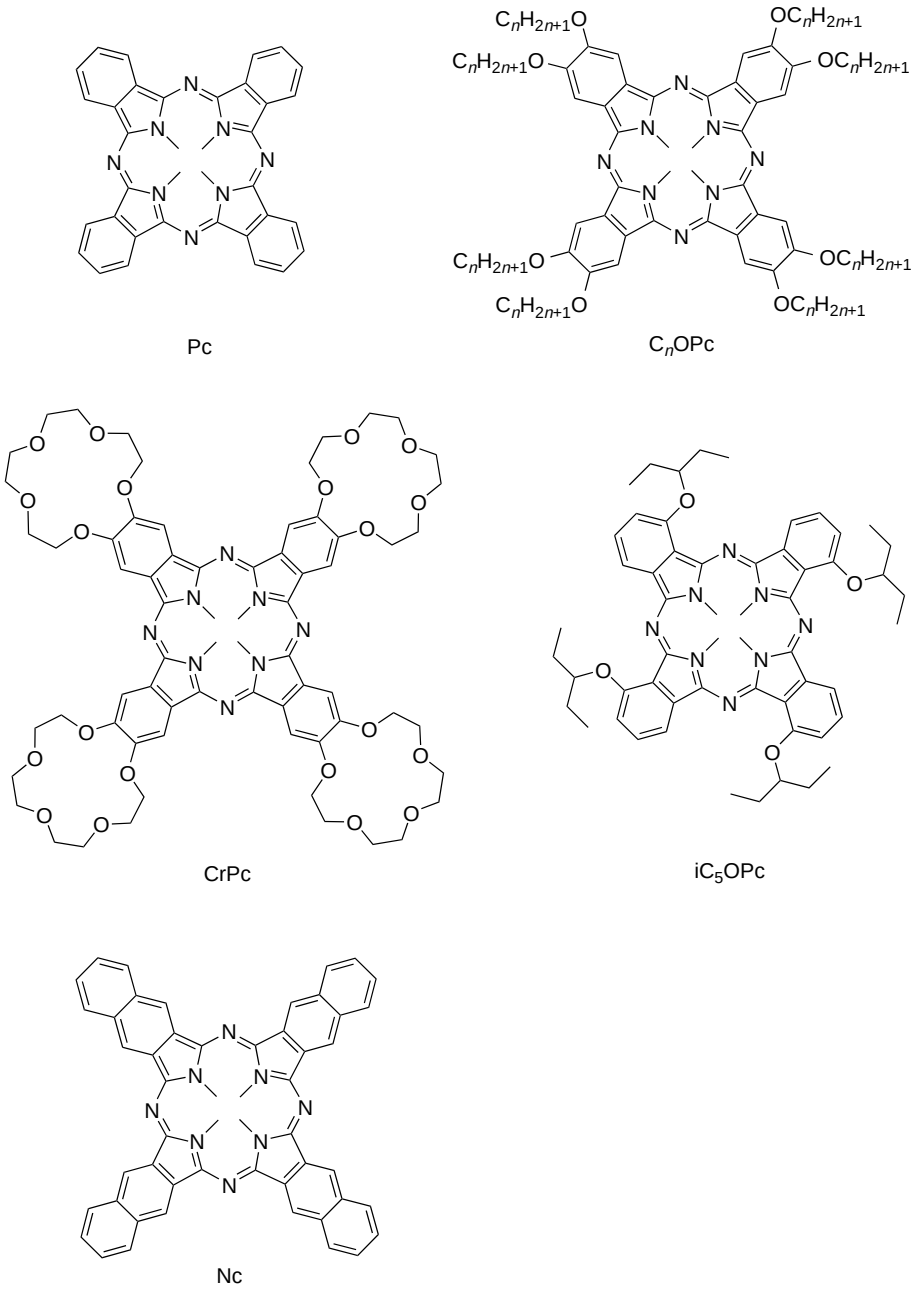

Figure 2. Phthalocyanine and naphthalocyanine units used in double- and triple-decker complexes.

2.1 Self-assembly on HOPG: single-component assemblies

Single-molecule images of a double-decker complex were captured by means of STM by Liu and co-workers as early as in 1991 (*40*). They prepared the sample by dropping a dilute solution of $[Lu(Pc)_2]$ on a graphite surface, although they did not mention what solvent they used. Later in 1997, Jones and co-workers (*41*) observed three Langmuir–Blodgett (LB) monolayers of $[Lu(Pc)_2]$ fabricated on HOPG by means of STM obtaining lamellar structures with a periodicity of 1.5 nm. It was difficult, however, to assign the observed features to the molecular structures due to limited resolution. They also carried out scanning tunnelling spectroscopy (STS) experiments and observed (i) a nonlinear, rectifying behaviour and (ii) small peaks in the *I*/*V* curve near -600 mV (substrate potential with respect to the tip). An analogue decorated with short hydrocarbon chains, $[Lu(C_4OPc)_2]$, also gave some distinct structures, but reproducible scanning was more difficult than for $[Lu(Pc)_2]$. Thermal deposition of $[Ti(Pc)_2]$ on the HOPG surface resulted only in disordered coverage of the surface by the complexes (*38*).

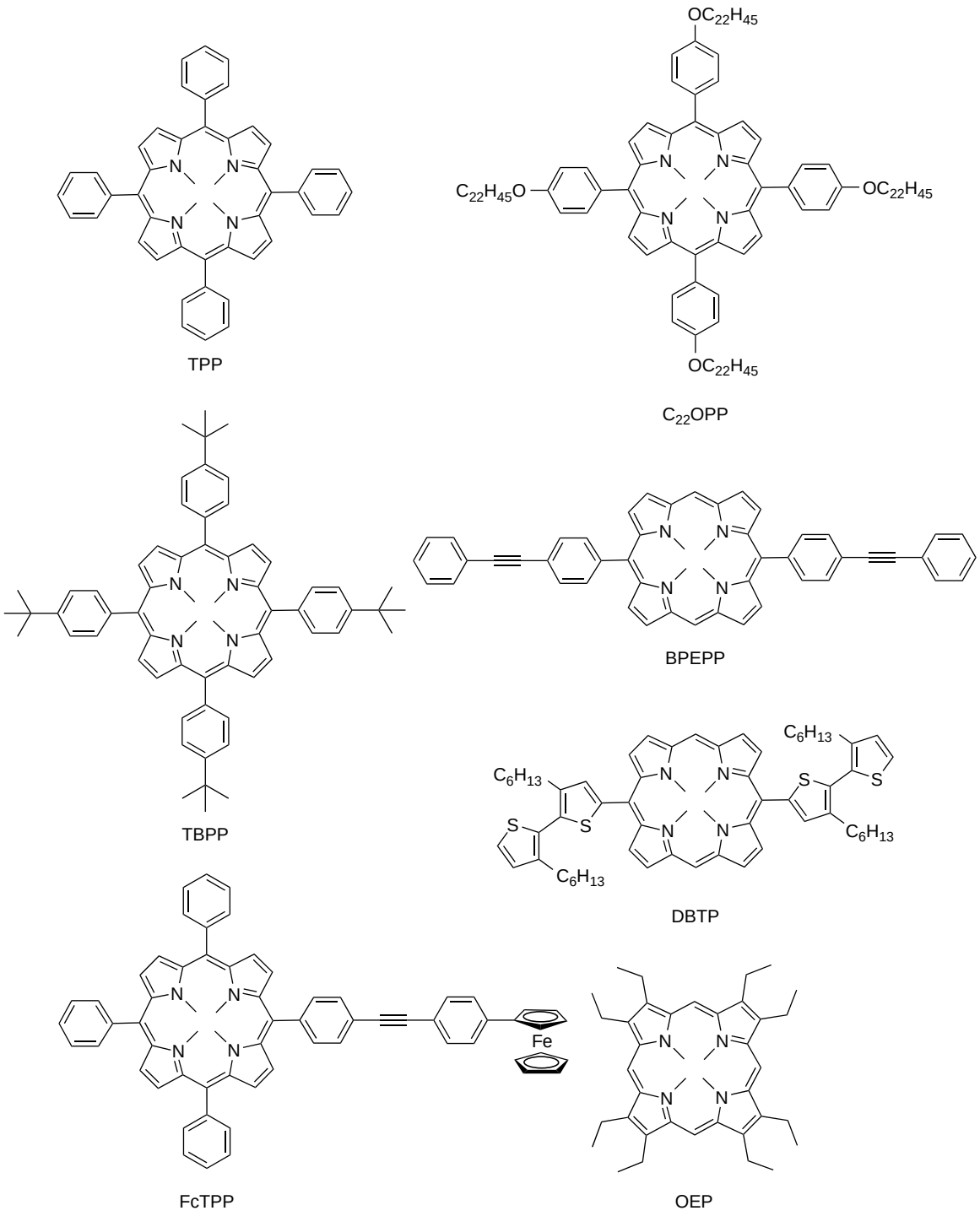

Figure 3. Porphyrin units used in double- and triple-decker complexes.

To immobilise a molecule on the surface of HOPG, attaching long hydrocarbon chains is a powerful strategy, because of a high affinity of hydrocarbon chains towards the HOPG surface (*9*). Thus, octa(alkoxy)phthalocyanines form 2D-ordered arrays on the HOPG surface with the hydrocarbon chains being interdigitated. Miyake and co-workers (*42*) examined the influence of the length of hydrocarbon chains on the assembly structures for monomeric phthalocyanines, $H_2(C_nOPc)$, where $n = 4–18$. Their results at the interface of HOPG–1-phenyloctane indicates that $H_2(C_4OPc)$ forms a square lattice (1.9 nm × 1.9 nm); $H_2(C_8OPc)$ forms both square and

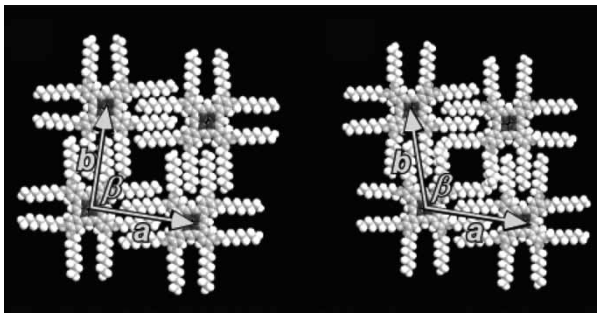

Figure 4. Proposed models of interdigitation of hydrocarbon chains of $H_2(C_8OPc)$. Left: $a = 2.6(0.1)$ nm, $b = 2.6(0.2)$ nm, $\beta = 92(4)°$; right: $a = 2.6(0.1)$ nm, $b = 2.6(0.2)$ nm, $\beta = 106(2)°$. Reprinted with permission from (*42*). Copyright 2008 American Chemical Society.

hexagonal lattices (2.6 nm × 2.6 nm) evenly; and $H_2(C_{12}OPc)$ forms predominantly a hexagonal lattice (3.4 nm × 3.4 nm). Although the hydrocarbon chains are rarely observed with STM, possible models have been proposed to account for the arrangement of the molecules, which are displayed for $H_2(C_8OPc)$ in Figure 4. The surface density is higher in the hexagonal lattice than in the square lattice by 13%.

Similarly, bis(phthalocyanine) sandwich complexes with long hydrocarbon chains form ordered arrays. 2D lattices formed from a series of double-decker complexes bearing C_nOPc as a bottom ligand, where $n = 4$, 8, 12, are summarised in Table 2, together with the values for the monomeric units, $H_2(C_nOPc)$. As of $n = 4$, $[Tb(C_4OPc)_2]$ forms a square lattice nearly identical to that of $H_2(C_4OPc)$ (*43*).

As of $n = 8$, monomeric ligand, $H_2(C_8OPc)$, is ambivalent in that it forms both square and hexagonal domains evenly, which shows that these phases have similar stabilities. The double-decker complexes, $[M(C_8OPc)_2]$, also form both square and hexagonal lattices, but the former predominates (*44–46*). This could be attributed to steric effects of the upper ligand, because the density of the square lattice is lower than that of the hexagonal lattice, as previously mentioned. Especially, it would be difficult for the hydrocarbon chains of the upper disc to be properly accommodated because of the twist of 45° with respect to the lower disc, of which the hydrocarbon chains already form optimum interdigitated packing structures. However, repulsion between the hydrocarbon chains may not be the only reason for the preference of the square lattice, because double-decker complexes without hydrocarbon chains in the upper disc, [M(Pc)(C_8OPc)], also prefer square lattices over hexagonal lattices (*44*, *47*). A larger upper disc exerts a more explicit impact on the lattice formed. The double-decker complex bearing a Nc ligand, [Lu(Nc)(C_8OPc)], forms a square lattice but with a larger lattice constant of 3.0 nm than that of $H_2(C_8OPc)$ (*47*). The expanded lattice has been attributed to steric interactions between the hydrocarbon terminals and the outer edge of the upper disc.

As of $n = 12$, $H_2(C_{12}OPc)_2$ forms a hexagonal lattice predominantly, at the HOPG–1-phenyloctane interface (*42*). It is reported, however, that it forms a square lattice at the interface of HOPG–1,2,4-trichlorobenzene (*48*). This dependence on the solvent is translated into double-decker complexes: hexagonal lattices were reported for $[Ce(C_{12}OPc)_2]$ and $[Er(C_{12}OPc)_2]$ in 1-phenyloctane (*44*), while

Table 2. Lattices of $H_2(C_4OPc)$ and $[M(C_nOPc)_2]$ formed on HOPG.

Compounds	Conditions	Lattices	Lattice constants (nm × nm, degree)	Ref.
$H_2(C_4OPc)$	1-Phenyloctane	Square	1.9(0.1) × 1.9(0.1), 92(2)	(*42*)
$[Tb(C_4OPc)_2]$	Air	Square	2 × 2	(*43*)
$H_2(C_8OPc)$	1-Phenyloctane	Square	2.6(0.1) × 2.6(0.2), 92(4)	(*42*)
		Hexagonal	2.6(0.1) × 2.6(0.2), 106(2)	(*42*)
$[Ce(C_8OPc)_2]$	1-Phenyloctane	Square	2.7(0.3) × 2.7(0.3), 92(4)	(*44*)
		Hexagonal (minor)		(*44*)
$[Lu(C_8OPc)_2]$	1-Phenyloctane	Pseudo-square	2.5(0.1) × 2.7(0.1), 83(5)	(*45*)
		Hexagonal	2.6(0.1) × 2.6(0.1)	(*45*)
$[Pr(C_8OPc)_2]$	1-Phenyloctane	Square	2.6(0.2) × 2.6(0.2), 89(2)	(*46*)
		Hexagonal (minor)	2.4(0.2) × 2.5(0.2), 57(2)	(*46*)
[Ce(Pc)(C_8OPc)]	1-Phenyloctane	Square (dominant)	'identical to... $H_2(C_8OPc)$'	(*44*)
[Lu(Pc)(C_8OPc)]	1-Phenyloctane	Square	2.5(0.1) × 2.5(0.1)	(*47*)
[Lu(Nc)(C_8OPc)]	1-Phenyloctane	Square	3.0(0.1) × 3.0(0.1)	(*47*)
$H_2(C_{12}OPc)$	1-Phenyloctane	Hexagonal	3.4(0.3) × 3.4(0.3), 117(8)	(*42*)
$H_2(C_{12}OPc)$	1,2,4-Trichlorobenzene	Square	2.9(0.1) × 2.9(0.1), 90(5)	(*48*)
$[Ce(C_{12}OPc)_2]$	1-Phenyloctane	Hexagonal	3.5(0.3) × 3.5(0.3), 124(10)	(*44*)
		Square (minor)	3.2(0.2) × 3.2(0.2), 93(4)	(*44*)
$[Er(C_{12}OPc)_2]$	1-Phenyloctane	Hexagonal	3 × 3	(*49*)
$[Er(C_{12}OPc)_2]$	1,2,4-Trichlorobenzene	Square	3.0(0.1) × 3.0(0.1), 90(3)	(*48*)

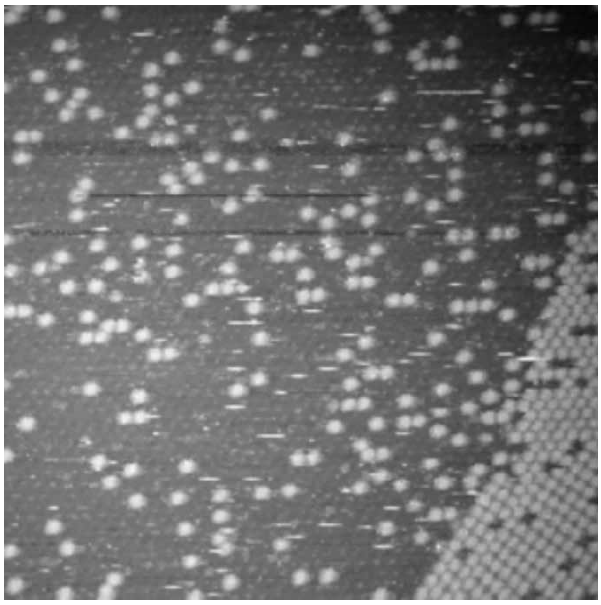

Figure 5. 2D gas and solid phases of $[Lu(C_8OPc)_2]$ at the HOPG–1-phenyloctane interface; $100 \times 100\,nm^2$. Reprinted with permission from (*45*). Copyright 2006 American Chemical Society.

a square lattice was reported for $[Er(C_{12}OPc)_2]$ in 1,2,4-trichlorobenzene (*49*). The effects of the solvent on the resulting assembly structure are not fully understood.

Remarkably, a STM image captures not only the 2D crystal phase but also a 2D gas phase of $[Lu(C_8OPc)_2]$, as shown in Figure 5. A crystalline phase is seen at the lower right corner of the image, while the molecules are scattered around in a 2D gas phase in the remaining regions of the image. Note that there is another monolayer underneath these crystalline and gas phases; the solid and gas phases are in the second layer from the substrate surface.

Takami and co-workers (*50*) investigated the surface arrangement of a series of double-decker complexes of lutetium containing a naphthalocyanine unit as one of the ligands, [Lu(OEP)(Nc)], [Lu(TBPP)(Nc)] and $[Lu(iC_5OPc)(Nc)]$. All three complexes form ordered arrays with a common lattice constant of 1.7 nm, which matches the optimised arrangement of naphthalocyanine, indicating that the Nc unit adsorbs on the surface, presenting the other ligand off the surface towards the solution.

Tetraphenylporphyrins modified with long hydrocarbon chains also form 2D-ordered arrays at HOPG–solution interfaces. These porphyrins form lamellar

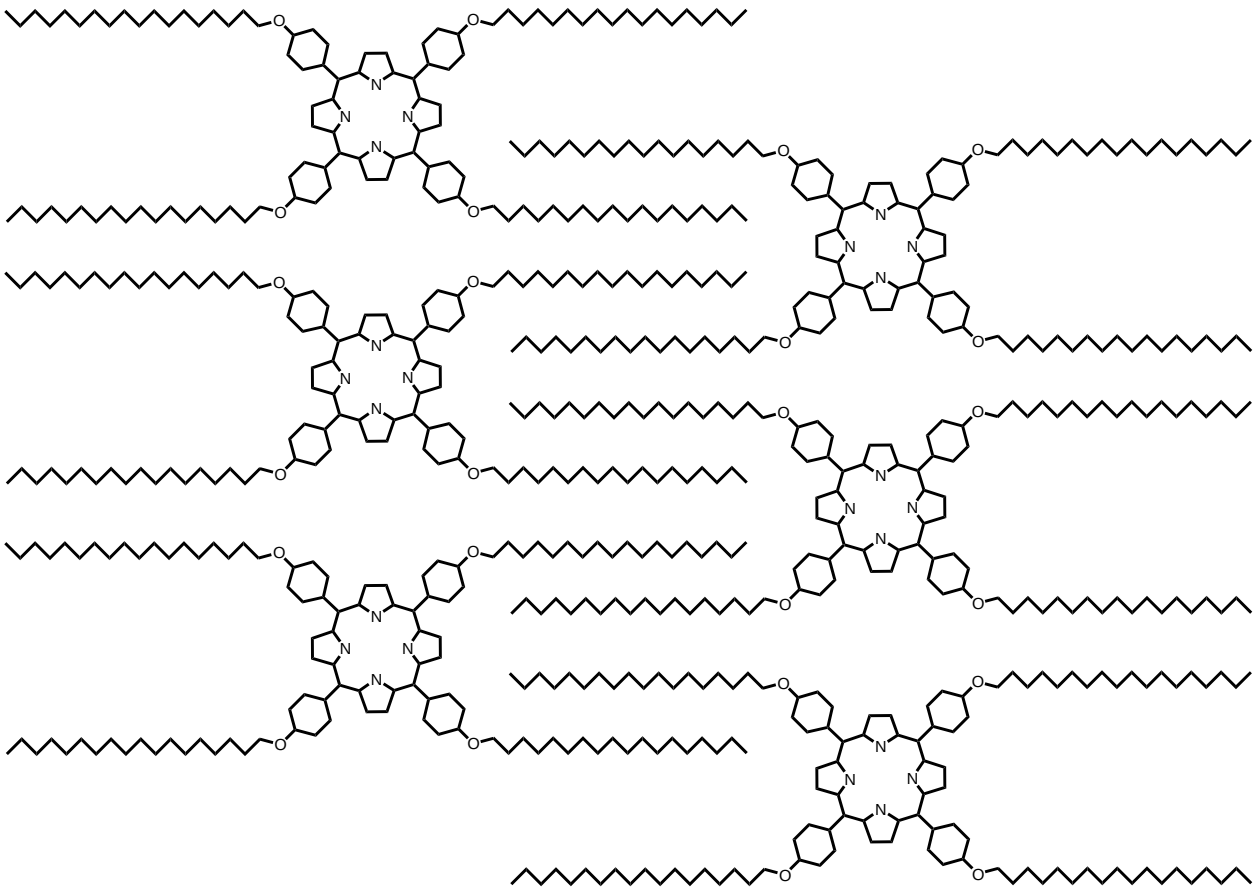

Figure 6. Schematic surface arrangement of tetraphenylporphyrin modified with long hydrocarbon chains.

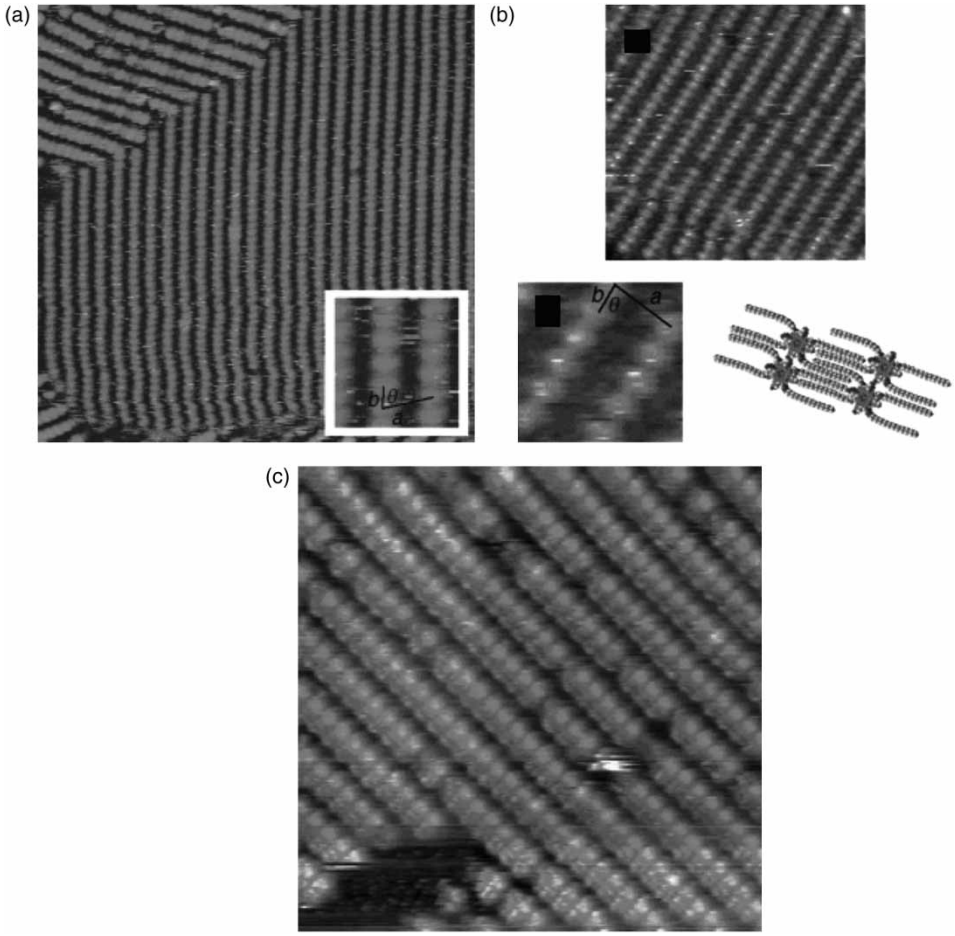

Figure 7. STM images of porphyrin arrays at the HOPG–1-phenyloctane interface. Reprinted with permission from (*51*). Copyright 2006 American Chemical Society. (a) [Ce(Pc)(C_{22}OPP)]; $100 \times 100\,nm^2$; inset: $10 \times 10\,nm^2$. (b) [Ce(C_{22}OPP)$_2$]; top: $50 \times 50\,nm^2$; lower left: $10 \times 10\,nm^2$; lower right: molecular models. (c) [Ce(BPEPP)(C_{22}OPP)]; $50 \times 50\,nm^2$.

structures, the hydrocarbon chains from across the rows being interdigitated as shown in Figure 6. We have revealed that the double-decker porphyrin complexes that have a C_{22}OPP ligand, i.e. [Ce(Pc)(C_{22}OPP)], [Ce(C_{22}OPP)$_2$] and [Ce(BPEPP)(C_{22}OPP)], assemble themselves into nearly identical motifs to that of H_2(C_{22}OPP), which indicated that the alkylated porphyrins are adsorbed on the surface, determining the surface arrangement (Figure 7) (*51*). It is interesting to note that the shapes of the bright features observed in the STM images differ depending on the upper ligand: the Pc ligand gave a circular shape (Figure 7(a)); the C_{22}OPP ligand gave a square shape (Figure 7(b)); and the BPEPP ligand gave an elliptic shape (Figure 7(c)). The orientation of the squares for [Ce(C_{22}OPP)$_2$] is informative. Assuming that the four corners of the square correspond to the four *meso*-phenylene groups, the observed orientation indicates that the upper porphyrin ring is rotated by 45° with respect to the lower porphyrin ring. This is a manifestation of the anti-prismatic coordination geometry of double-decker sandwich complexes in general. The bright elliptic features in the image of [Ce(BPEPP)(C_{22}OPP)] are oriented perpendicular to the molecular rows. We believe that these features correspond to the elliptic shape of the upper BPEPP ring. The distance between the terminal hydrogens on both ends of the BPEPP unit is 3.16 nm, well over the intermolecular distance along the molecular row, which is 2.0 nm. Hence, the BPEPP unit is forced to orient perpendicular to the molecular row. The perpendicular orientation is accommodated, because the interlamellar separation is large enough, 4.44 nm.

2.2 Self-assembly on HOPG: multi-component assemblies

As we have seen above, almost in all the cases, double-decker sandwich complexes assemble with one of the ligands being parallel to the surface. The surface arrangement is determined by the arrangement of the adsorbed, bottom ligand with a slight modification effected by the top ligand. As a next step towards constructing more complex surface assemblies, it would

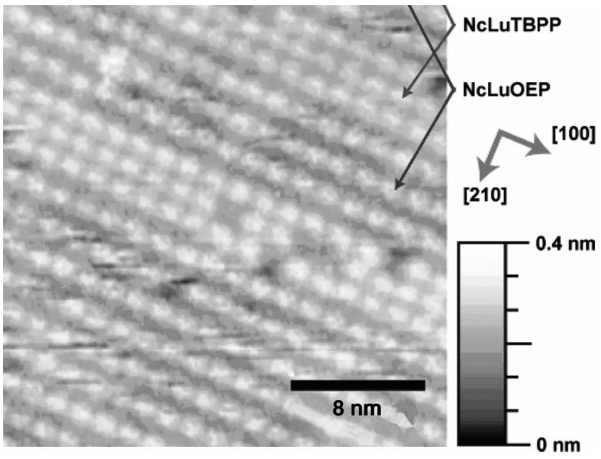

Figure 8. [Lu(OEP)(Nc)] and [Lu(TBPP)(Nc)] form segregated bundles. Reprinted with permission from (*50*). Copyright 2007 American Chemical Society.

be interesting to examine the arrangement of mixtures of a double-decker complex with a monomeric phthalocyanine or porphyrin compound. There are some possible arrangements for such mixtures: the two components could randomly mix with each other because the lattice is nearly identical; the two components could be separated into different phases due to some effects exerted by the top ligand; or the two components mix with a certain regularity leading to new surface patterns.

Mixtures of [Er($PcOC_{12}$)$_2$] and [Co(C_{12}OPc)] exhibited some phase separation, even though they have the identical lattice parameters (*48*). This fact confirms that not only the bottom ligand but also the top ligand has an effect on the assembly structure. Mixtures of [Er(C_{12}OPc)$_2$] and [Co(C_8OPc)], with different hydrocarbon chains, resulted in clear phase separation, as expected. An interesting case of phase separation is found for a mixture of [Lu(OEP)(Nc)] and [Lu(TBPP)(Nc)] (*50*). The lattice constants for these complexes are identical, with the unit cell of 1.7 nm. Still, they segregate to form different bundles of rows as shown in Figure 8. The brighter protrusions are of [Lu(TBPP)(Nc)] and the darker protrusions are of [Lu(OEP)(Nc)].

More distinct superstructures were formed when [Ce(C_8OPc)$_2$] and [Ce(Pc)(C_8OPc)] were mixed with the monomeric counterpart, H_2(C_8OPc) (*44*). For mixtures of [Ce(C_8OPc)$_2$] and H_2(C_8OPc) (Figure 9(a)), these molecules tend to align alternately in a chessboard pattern, although many local varieties exist. Two distinct patterns were found for mixtures of [Ce(Pc)(C_8OPc)] and H_2(C_8OPc). In one pattern, the ratio of [Ce(Pc)(C_8OPc)] and H_2(C_8OPc) is 1:3 (Figure 9(b), left). In the other, the ratio is 1:1 and the double-decker molecules and the monomer molecules make alternate rows (Figure 9(b), right). A reason for the formation of these patterns, apparently, is to avoid steric crowding between the top ligands of the double-decker complexes. However, some cooperativity should be in operation through the bottom ligand or hydrocarbon chains because the regularity arises even though no direct inter-top-ligand interactions are possible.

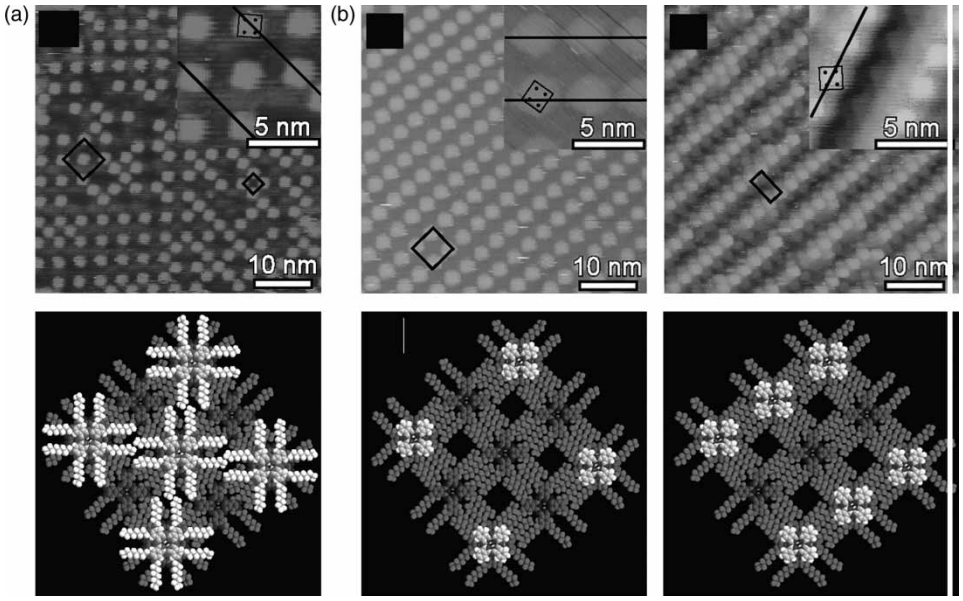

Figure 9. Mixtures of a sandwich complex and its monomer counterpart form distinct motifs. Reprinted with permission from (*44*). Copyright 2009 American Chemical Society. (a) [Ce(C_8OPc)$_2$] and H_2(C_8OPc). (b) Two kinds of superstructures observed for mixtures of [Ce(Pc)(C_8OPc)] and H_2(C_8OPc).

2.3 Self-assembly on Au(111)

Several methods were employed for the deposition of double-decker complexes onto the surface of gold crystals, including vacuum deposition, a pulse injection method and deposition from solution.

$[Y(C_8OPc)_2]$ and $[Ce(C_8OPc)_2]$ were deposited from a benzene solution onto Au(111) and were studied at an electrochemical interface in a 0.1 M $HClO_4$ solution (*52*). $[Y(C_8OPc)_2]$ adlayer thus prepared forms mostly a rectangular lattice, with lattice constants of 2.31 and 2.50 nm, along the $[\bar{1}10]$ and $[\bar{1}\bar{1}2]$ directions, respectively. The 2D crystals form some domains of which orientations are mutually related by 60°. These data indicate that the molecular arrangement is correlated with the substrate orientation. The structure of the molecular assemblies depended on the substrate potential, which can be controlled independently from the bias potentials in the electrochemical STM configuration. In short, the mobility of adsorbed molecules is large at negative potentials, whereas the binding to the surface is too strong for the molecules to form ordered assemblies at positive potentials. Optimum potential range for the ordered assembly formation was found, for this particular double-decker complex, to be +0.2 to +1.0 V vs. reversible hydrogen electrode (RHE). $[Ce(C_8OPc)_2]$ formed a rectangular lattice similar to that of $[Y(C_8OPc)_2]$.

The monolayer formation on the Au(111) affects the properties of the surface in terms of both the structure and electron transfer behaviour. As for the structure, the adlayer formation lifted the reconstruction of the Au(111) surface, that is, the formation of the well-known $22 \times \sqrt{3}$ structure was suppressed. More interestingly, the monolayer formation appears to facilitate electron transfer reaction between the electrode (Au(111)) and Fe(III)/Fe(II) ions in solution. The promotion of electron transfer was manifested in more reversible waves recorded in cyclic voltammetry and linear relations in the Nyquist impedance spectra. It was thought that the acceleration of the electron transfer is due to prevention of the perchlorate anion (and other unknown species) from adsorbing to the surface and redox properties of these double-decker complexes, which have redox potentials near the Fe(III)/Fe(II) couple.

The non-alkylated analogue of $[Y(C_8OPc)_2]$, $[Y(Pc)_2]$, was thermally deposited on Au(111) (*53*). The double-decker complex was imaged as an eight-lobed structure by means of ultra-high vacuum (UHV) STM at 4.8 K as shown in Figure 10(a). The authors proposed that the eight-lobed bright parts correspond to the sides of the benzene rings on the upper Pc core of the double-decker complex. The adsorption orientation is determined by the lower Pc ring, the diagonal axis of which aligns parallel to the close-packed, $[\bar{1}10]$ direction (or equivalent $[0\bar{1}1]$ and $[\bar{1}01]$ directions) of the Au substrate. As the upper ring rotates with respect to the lower ring by 45°, the diagonal axis of the upper ring is also rotated from the $[\bar{1}10]$ direction of the gold substrate.

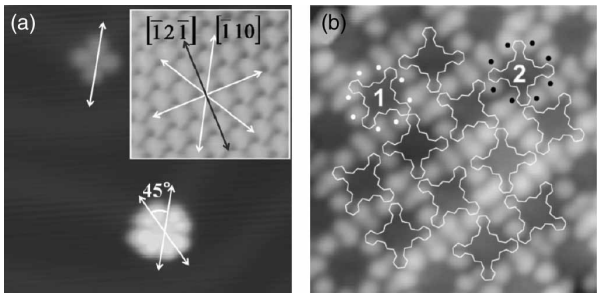

Figure 10. STM images of $[Y(Pc)_2]$ on Au(111) at 4.8 K. Reprinted with permission from (*53*). Copyright 2009 American Chemical Society. (a) Isolated molecules ($11 \times 11\,nm^2$). The brighter eight-lobed feature and the darker four-lobed feature correspond to $[Y(Pc)_2]$ and a Pc molecule, respectively. (b) 2D crystals ($6.4 \times 6.4\,nm^2$). Numbers 1 and 2 mark two different orientations. Dots highlight that the bright features are positioned at the sides of the benzene rings.

Figure 10(b) shows the morphology of a more condensed 2D film. The bright features are assigned to the sides of the four benzene rings of the upper Pc ring as in the case of an isolated complex. It is noted that the neighbouring upper rings are alternately rotated by ~30°; the respective orientations are marked 1 and 2 in the figure. Both of the orientations can be accounted for assuming that the diagonal axis of the lower Pc ring aligns parallel to the close-packed directions of the Au(111) substrate. The alternate variation in the orientation indicates that two out of the three equivalent orientations of the lower Pc rings are alternately chosen. Thus, intermolecular interactions lift the degeneracy of the three orientations.

A pulse injection method was employed to deposit a triple-decker complex, $[Ce_2(DBTP)_3]$, on the Au(111) surface (*54*). The pulse injection method has been developed to deposit large molecules for which thermal deposition is not feasible (*55–57*). The triple-decker complexes are mostly aligned along the herringbone structures of the reconstructed Au(111) surface.

2.4 Terbium phthalocyanine double-decker complexes as single-molecule magnets

Ishikawa and co-workers (*37*) have discovered that the terbium phthalocyanine double-decker complex, $Bu_4N^+ \cdot [Tb(Pc)_2]^-$, is qualified as a single-molecule magnet. Unlike other molecular magnets based on 3d metals, the magnetism arises solely from a single terbium atom. The Tb^{3+} ion has eight 4f electrons and hence the quantum number for the spin angular momentum is ($S =$) 3 and the orbital angular momentum is ($L =$) 3, which makes the total angular momentum ($J =$) 6. Within the double-decker complex, the ligand field splits the ground

multiplet so that the lowest sublevel has the largest J_z value of ± 6. The spin state, say, $J_z = +6$, is resistant to interconversion to the state $J_z = -6$ at low temperatures, because the second sublevel lies significantly above the ground level by $400\,\mathrm{cm}^{-1}$.

One of the difficulties, among others, in developing practical applications of single-molecule magnets is to address individual or small numbers of molecular magnets. Thus, it is necessary to fabricate thin oriented films of single-molecule magnets. Gómez-Segura et al. (*43*) obtained ordered arrays of $[Tb(C_4OPc)_2]$ on HOPG on drop-casting of a toluene solution and subsequent evaporation. The double-decker complex, as many other analogues, formed well-ordered arrays with face-on orientation. The preferential magnetisation axis of the 2D film is perpendicular to the substrate surface because the axis is along the C_4 axis of $[Tb(C_4OPc)_2]$.

The double-decker complex, $[Tb(Pc)_2]$ (as well as $[Dy(Pc)_2]$ and $[Y(Pc)_2]$), were thermally deposited on Au(111) (*58*). Both four-lobed and eight-lobed structures were observed with UHV-STM at 4.7 K. The former correspond to $H_2(Pc)$ or Tb(Pc), which is probably formed during the evaporation process, and the latter correspond to intact $[Tb(Pc)_2]$ molecules.

The same molecule was also deposited on Cu(111) using a dry-imprinting method and was studied with UHV-STM at 10 K (*39*). The energy-resolved conductance maps revealed the density of states in regard to energy and positions within the molecule. The obtained images are displayed in Figure 11(a); the higher electron density at a chosen energy is displayed in lighter colour. The data indicate that the electrons in levels at $+0.8$ and -0.8 eV are delocalised over the ligands, while those at 0.4 eV are centred on the Tb atom. The maps are in very good agreement with the results obtained by density functional theory (DFT) calculations, which are shown in Figure 11(b).

DFT calculations indicated that the neutral $[Tb(Pc)_2]$ molecule has two spin systems: one localised on the metal centre carrying a magnetic moment of 5.9 μ_B, where μ_B is the Bohr magneton, and the other delocalised over the two Pc ligands. The calculations also indicated that the spin system localised on the Tb centre is unaffected even upon strong adsorption on surfaces.

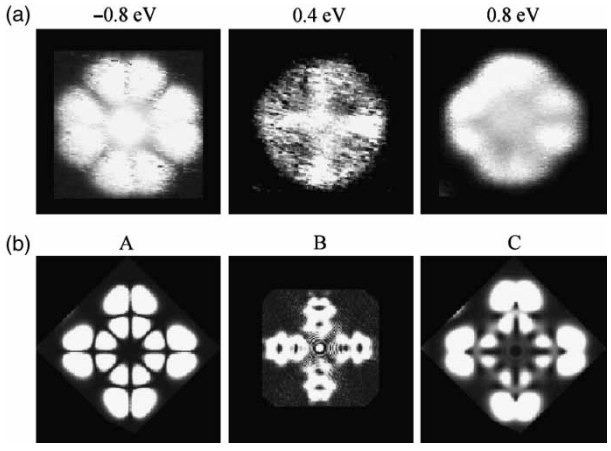

Figure 11. Energy-resolved conductance maps of the $[Tb(Pc)_2]$. Reprinted with permission from (*39*). Copyright 2008 American Chemical Society. (a) Obtained from STS. (b) Calculated with DFT.

3. Dynamic motion of double- and triple-decker complexes

3.1 *Potential-induced flip-flop*

Assemblies of an asymmetrical triple-decker complex, [(CrPc)Lu(CrPc)Lu(C_8OPc)], were investigated at the HOPG–1-phenyloctane interface (*59*, *60*). DFT calculations indicated that the complex has an intrinsic dipole moment of 17.5 D along the C_4 axis pointing from the CrPc end towards the C_8OPc end, although the origin of the dipole may not be obvious considering the similar alkoxy substituents on the Pc cores. The complex forms a well-ordered square lattice with a lattice constant of 2.6 nm at the interface of HOPG–1-phenyloctane, when observed with negative substrate bias potentials (Figure 12(a)). The lattice constant is similar to that reported for monomeric metallo and free-base phthalocyanines with the same set of hydrocarbon chains, [M(C_8OPc)]. The double-decker complex, $[Eu(CrPc)_2]$, also forms a square lattice but with a smaller lattice

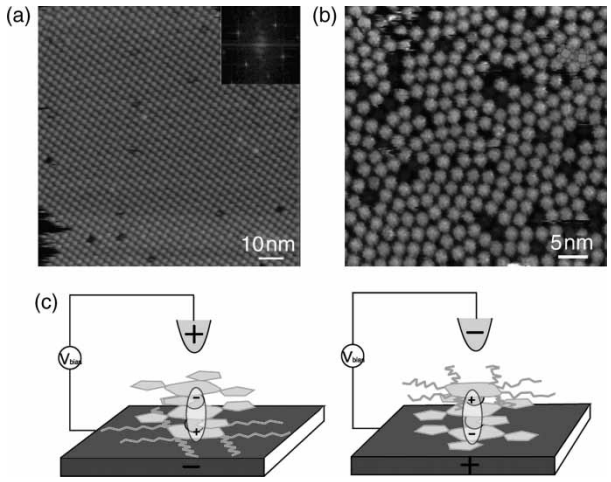

Figure 12. Bias-induced switching of the orientation and assembly of [(CrPc)Lu(CrPc)Lu(C_8OPc)] at the HOPG–1-phenyloctane interface. Reprinted with permission from (*59*). Copyright 2008 American Chemical Society. (a) Ordered assembly observed under a substrate bias potential of -0.50 V. (b) Disordered assembly observed under a substrate bias potential of $+1.50$ V. (c) Proposed flips of molecular orientation in response to the bias potential.

constant of 2.3 nm. Hence, it is likely that the triple-decker complex, [(CrPc)Lu(CrPc)Lu(C_8OPc)], adsorbs with the C_8OPc ligand facing towards the HOPG substrate, with the hydrocarbon chains interdigitated. In contrast, disordered assemblies were observed under positive substrate bias potentials (Figure 12(b)). Intermolecular distances are now distributed in a range of 2.3–2.8 nm. It was proposed that the molecule flips under a positive bias to the orientation in which the CrPc ligand faces towards the substrate surface, because of the interactions between the electric field and the molecular dipole moment (Figure 12(c)). Remarkably, the order–disorder transition induced by the molecular flip was reversibly controlled by the applied bias potentials. The dI/dV vs. V curves in the STS experiments exhibited a scan direction-dependent peak (*60*). The peak appeared at −1.1 V when the bias was scanned from positive to negative, while it appeared at +1.3 V when the bias was scanned from negative to positive. The authors attributed these peaks to the bias-polarity-induced flipping process of the molecules.

Yoshimoto and co-workers (*61*) investigated assemblies of another asymmetrical triple-decker complex, [(TPP)Eu(CrPc)Eu(CrPc)], at an electrochemical interface on Au(111). Assuming face-on adsorption of the complex onto the surface, there are two possible orientations of the molecules, i.e. those with a topmost TPP ligand and those with a topmost CrPc ligand. Upon deposition from a benzene solution under certain conditions, a well-organised rectangular chessboard pattern was observed at a substrate potential of +0.80 V vs. RHE. The chessboard pattern formed with spots of different heights arose from alternate adsorption orientations of the triple-decker complex. This chessboard pattern was completely replaced by another arrangement with spots of a uniform height at +0.02 V vs. RHE. A redox reaction occurs at 0.20 V vs. RHE during this potential modulation. Thus, it was demonstrated that the adsorption orientation and the structure of the assemblies were controlled by the redox states of the adsorbate triple-decker molecules.

3.2 Rotational libration of the macrocyclic ligand

Molecular rotors are attracting much attention in the pursuit of ever-smaller machines. The double-decker complexes may be considered among the most promising rotatable components for molecular rotors in view of their versatile functionalities and amenability to additional functionalisation. Studies in solution have revealed that the two macrocyclic rings undergo rational libration with respect to each other (*18*, *20*, *27–35*). Thus, visualisation of the rotational libration of double-decker complexes on an individual molecule basis is an important means of understanding the rotational dynamics and finding ways of controlling it.

Miyake and co-workers (*44*) discussed the motion of the top ligands in the arrays of double-decker complexes, by comparing the STM images of [Ce(C_8OPc)$_2$], [Ce(C_{12}OPc)$_2$], [Ce(Pc)(C_8OPc)] and [Ce(TPP)(C_8OPc)] (see Figure 9). Square contrasts were observed for the top Pc core in the cases of the former three complexes. This was the case even when the top ligands have enough space around them by being embedded in the matrix arrays of H_2(C_8OPc) or H_2(C_{12}OPc). On the other hand, the intramolecular feature was completely lost for the porphyrin complex, [Ce(TPP)(C_8OPc)]. One possible interpretation of these results may be that the top phthalocyanine ligand does not undergo rotation or any other significant movement, while the top porphyrin ligand undergoes some movements possibly including rotational libration and the trampoline-like movement.

The double-decker porphyrin complex with a porphyrin ligand with a two-fold symmetry, [Ce(BPEPP)(C_{22}OPP)], has been designed so that the orientation could be distinguished as mentioned previously (see Figure 7(c)). Figure 13 shows a mixed assembly of [Ce(BPEPP)(C_{22}OPP)] and H_2(C_{22}OPP). Brighter spots, [Ce(BPEPP)(C_{22}OPP)], and darker spots, H_2(C_{22}OPP), make up rows. In some regions, the double-decker complexes align consecutively, such as the region indicated by the bracket in the figure. In such places, the elliptic features orienting perpendicular to the row are observed. On the other hand, isolated double-decker

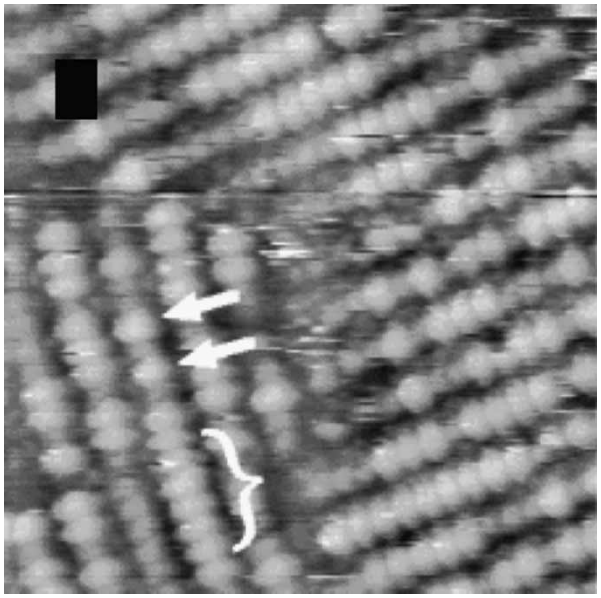

Figure 13. Assembly of a mixture of [Ce(BPEPP)(C_{22}OPP)] and H_2(C_{22}OPP) at the interface of HOPG–1-phenyloctane ($50 \times 50\,nm^2$). Reprinted with permission from (*51*). Copyright 2006 American Chemical Society. The arrows indicate isolated double-decker complexes, and the bracket indicates a row of double-decker complexes.

complexes, such as the ones indicated by the arrows in the figure, appear more or less isotropic. Rotational movement was invoked to rationalise the isotropic shape, as this complex undergoes interring rotational libration at a rate of $\sim 3\,s^{-1}$ in solution as revealed by temperature-variable ^1H NMR spectroscopy.

Clear evidence for rotational libration of a double-decker complex came from STM observation of [Ce(FcTPP)(C_{22}OPP)] by us (*62*). This complex was designed to have one extended arm terminated with a ferrocene unit on the TPP core. Thus, if the arm is visible with STM, it can function as a molecular beacon signalling its position. As a consequence, the four anti-prismatic orientations can be distinguished. The arm including a ferrocene unit was indeed visible in STM, as the image in Figure 14(a) shows. The linear rows of large spots in the image correspond to the double-decker cores, while smaller dots accompanying either on the left or on the right

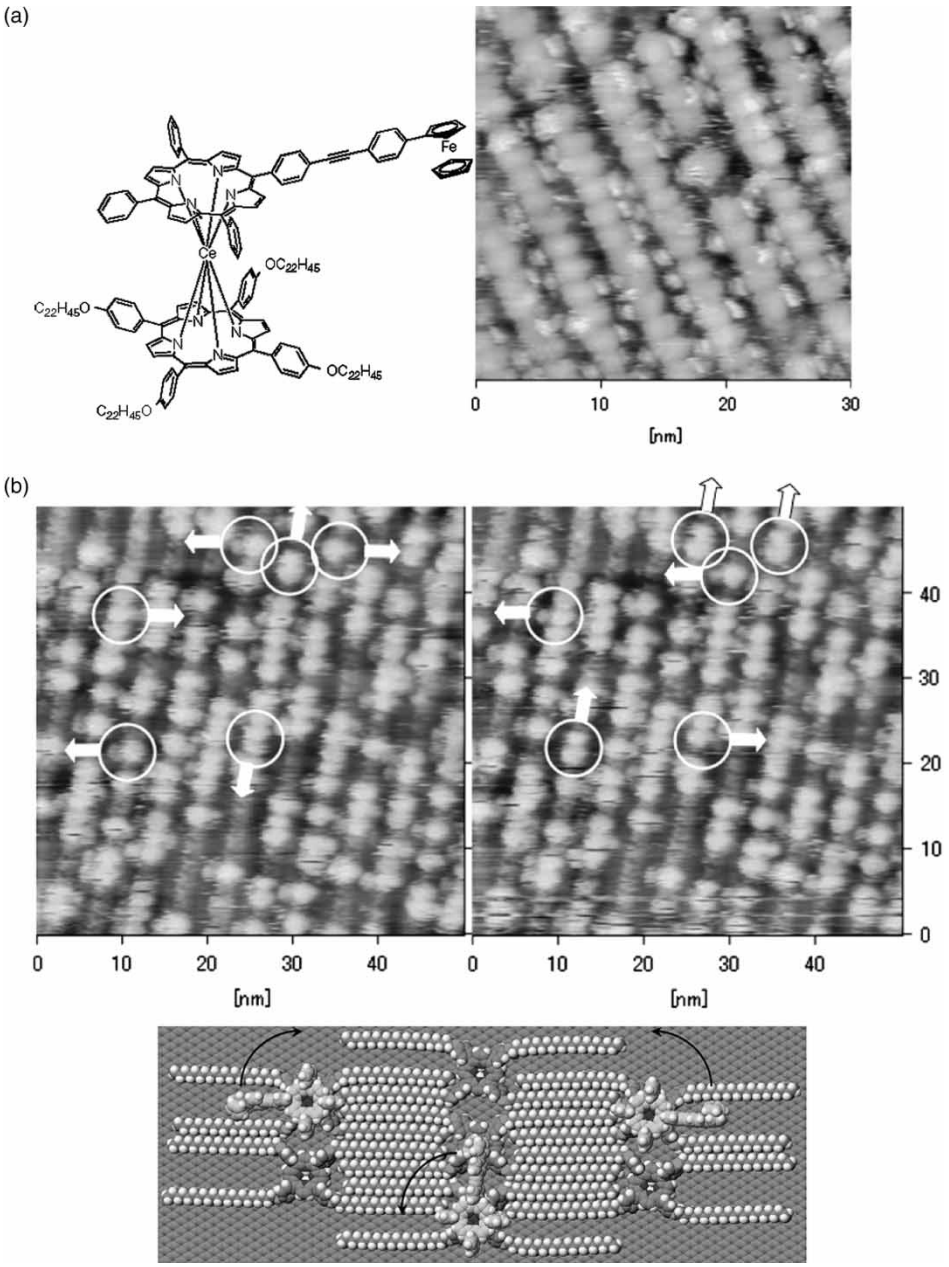

Figure 14. Assemblies of [Ce(FcTPP)(C_{22}OPP)] at the HOPG–1-phenyloctane interface. Reprinted with permission from (*62*). Copyright 2010 American Chemical Society. (a) Chemical structure and the 2D assembly of [Ce(FcTPP)(C_{22}OPP)]. (b) STM images of the same area of 2D assembly of a mixture of [Ce(FcTPP)(C_{22}OPP)] and H_2(C_{22}OPP); the right image was recorded immediately after (starting 86 s later) the left image. Encircled molecules changed their orientation during the interval; arrows indicate the orientation of the ferrocene units. The bottom illustration shows the three-circled units in the upper regions of the images.

side of the rows correspond to the arms. In the lamellar assembly, all the arms orient perpendicular to the row due to steric reasons.

STM images of a mixture of [Ce(FcTPP)(C_{22}OPP)] and H_2(C_{22}OPP) reveal molecules aligned in the same manner as those in the cases of [Ce(FcTPP)(C_{22}OPP)] alone. We ascribe the dimmer spots on the rows to the free-base porphyrin. Many of the brighter spots are accompanied by a smaller feature located on either the left or the right side. These pairs correspond to double-decker porphyrins in a perpendicular orientation. Some brighter spots form a pair on the row without being accompanied by a feature on the left or right side, which are assigned as double-decker porphyrins with a parallel orientation. The right-hand image in Figure 14(b) was recorded immediately after (starting 86 s later) recording that on the left image. Comparison of these two images revealed that most of the double-decker complexes stayed in the same orientation, some had reoriented between the first and second scans, which are encircled in the figure with arrows indicating their orientations. The reorientations of the three units grouped in the upper regions of the images are illustrated schematically in the lower panel. Thus, we have visualised the orientational change of double-decker complexes in real space on an individual molecule basis.

Analysis by counting molecules revealed that the rate of rotational libration (a 90° flip) is in a range of 10^{-3} and $10^{-2}\,s^{-1}$. The rate is influenced by its direction, i.e. perpendicular to parallel or vice versa, and whether the neighbouring molecules are [Ce(FcTPP)(C_{22}OPP)] or H_2(C_{22}OPP). Thus, the effects of specific environments of individual molecules on the molecular motion have been revealed.

4. Conclusion and prospects

Double- and triple-decker complexes form well-organised assemblies on surfaces. One of the macrocyclic ligands adsorbs on the surface almost always in a face-on manner. Long hydrocarbon chains are helpful for the assembly on the surface of HOPG. Either on HOPG or on Au(111), not only the bottom ligand but also the top ligand affects the resulting structures. Further introduction of directional interaction sites, such as hydrogen bonding sites and coordination sites, into the molecular structures would be a promising approach to construct more elaborate 2D assemblies. Investigation into the electronic and magnetic properties of these complexes and their 2D assemblies is under way. Especially, magnetic properties of single-molecule magnets are a challenging theme to be probed. Exploration of the rotatory motions of the ligands is in progress as well. Controlling the rotation of individual double-decker complexes and realising concerted rotation (molecular gears) may be challenging targets in the next step. Thus, double- and triple-decker complexes belong to a functional class of compounds that have intriguing properties in terms of structural, electronic, magnetic and, finally, dynamic points of view that might be useful for the development of molecular devices.

Acknowledgements

This work was supported by Grant-in-Aid for Scientific Research on Innovative Areas ('Coordination Programming' Area 2107, No. 22108532) and (C) (No. 21510104) from the Ministry of Education, Culture, Sports, Science and Technology, Japan and Nihon University '*N.*' Research Project.

References

(1) Ariga, K.; Hill, J.P.; Lee, M.V.; Vinu, A.; Charvet, R.; Acharya, S. *Sci. Technol. Adv. Mater.* **2008**, *9*, 014109.
(2) Ajayaghosh, A.; Praveen, V.K.; Vijayakumar, C. *Chem. Soc. Rev.* **2008**, *37*, 109–122.
(3) Yoshizawa, M.; Klosterman, J.K.; Fujita, M. *Angew. Chem. Int. Ed.* **2009**, *48*, 3418–3438.
(4) Giancarlo, L.C.; Flynn, G.W. *Acc. Chem. Res.* **2000**, *33*, 409–501.
(5) Frommer, J. *Angew. Chem. Int. Ed.* **1992**, *31*, 1298–1328.
(6) Barth, J.V.; Weckesser, J.; Lin, N.; Dmitriev, A.; Kern, K. *Appl. Phys. A* **2003**, *76*, 645–652.
(7) Yoshimoto, S. *Bull. Chem. Soc. Jpn.* **2006**, *79*, 1167–1190.
(8) Bonifazi, D.; Mohnani, S.; Llanes-Pallas, A. *Chem. Eur. J.* **2009**, *15*, 7004–7025.
(9) Cyr, D.M.; Venkataraman, B.; Flynn, G.W. *Chem. Mater.* **1996**, *8*, 1600–1615.
(10) De Feyter, S.; De Schryver, F.C. *Chem. Soc. Rev.* **2003**, *32*, 139–150.
(11) Ruben, M.; Lehn, J.-M.; Müller, P. *Chem. Soc. Rev.* **2006**, *35*, 1056–1067.
(12) Petukhov, K.; Alam, M.S.; Rupp, H.; Stroemsdoerfer, S.; Mueller, P.; Scheurer, A.; Saalfrank, R.W.; Kortus, J.; Postnikov, A.; Ruben, M.; Thompson, L.K.; Lehn, J.-M. *Coord. Chem. Rev.* **2009**, *253*, 2387–2398.
(13) Miyashita, N.; Kurth, D.G. *J. Mater. Chem.* **2008**, *18*, 2636–2649.
(14) De Feyter, S.; De Schryver, F.C. *J. Phys. Chem. B* **2005**, *109*, 4290–4302.
(15) Samorì, P.; Rabe, J.P. *J. Phys. Condens. Matter.* **2002**, *14*, 9955–9973.
(16) Yoshimoto, S.; Itaya, K. *J. Porphyr. Phthalocyanines* **2007**, *11*, 313–333.
(17) Otsuki, J. *Coord. Chem. Rev.*, **2010**, *254*, 2311–2341.
(18) Takeuchi, M.; Ikeda, M.; Sugasaki, A.; Shinkai, S. *Acc. Chem. Res.* **2001**, *34*, 865–873.
(19) Jiang, J.; Ng, D.K.P. *Acc. Chem. Res.* **2009**, *42*, 79.
(20) Shinkai, S.; Takeuchi, M. *Bull. Chem. Soc. Jpn.* **2005**, *78*, 40–51.
(21) Ng, D.K.P.; Jiang, J. *Chem. Soc. Rev.* **1997**, *26*, 433–442.
(22) Jiang, J.; Liu, W.; Arnold, D.P. *J. Porphyr. Phthalocyanines* **2003**, *7*, 459–473.
(23) Buchler, J.W.; Ng, D.K.P. In *The Porphyrin Handbook*; Kadish, K.M., Smith, K.M., Guilard, R., Eds.; Academic Press: San Diego, CA, 2000; Vol. 3, pp 245–294.
(24) Weiss, R.; Fischer, J. In *The Porphyrin Handbook*; Kadish, K.M., Smith, K.M., Guilard, R., Eds.; Elsevier Science: San Diego, CA, 2003; Vol. 16, pp 171–246.

(25) Jiang, J.; Kasuga, K.; Arnold, D.P. In Sandwich-type Phthalocyaninato and Porphyrinato Metal Complexes. *Supramolecular Photosensitive and Electroactive Materials*; Nalwa, H.S., Ed.; Academic Press: San Diego, CA, 2001; pp 113–210.
(26) Piechocki, C.; Simon, J.; André, J.-J.; Guillon, D.; Petit, P.; Skoulios, A.; Weber, P. *Chem. Phys. Lett.* **1985**, *122*, 124–128.
(27) Tashiro, K.; Konishi, K.; Aida, T. *Angew. Chem. Int. Ed. Engl.* **1997**, *36*, 856–858.
(28) Tashiro, K.; Fujwara, T.; Konishi, K.; Aida, T. *Chem. Commun.* **1998**, 1121–1122.
(29) Tashiro, K.; Konishi, K.; Aida, T. *J. Am. Chem. Soc.* **2000**, *122*, 7921–7926.
(30) Ikeda, M.; Takeuchi, M.; Shinkai, S.; Tani, F.; Naruta, Y. *Bull. Chem. Soc. Jpn.* **2001**, *74*, 739–746.
(31) Ikeda, M.; Takeuchi, M.; Shinkai, S.; Tani, F.; Naruta, Y.; Sakamoto, S.; Yamaguchi, K. *Chem. Eur. J.* **2002**, *8*, 5542–5550.
(32) Ikeda, M.; Kubo, Y.; Yamashita, K.; Ikeda, T.; Takeuchi, M.; Shinkai, S. *Eur. J. Org. Chem.* **2007**, 1883–1886.
(33) Ikeda, T.; Hirata, O.; Takeuchi, M.; Shinkai, S. *J. Am. Chem. Soc.* **2006**, *128*, 16008–16009.
(34) Sugasaki, A.; Ikeda, M.; Takeuchi, M.; Robertson, A.; Shinkai, S. *J. Chem. Soc. Perkin Trans. 1* **1999**, 3259–3264.
(35) Takeuchi, M.; Imada, T.; Ikeda, M.; Shinkai, S. *Tetrahedron Lett.* **1998**, *39*, 7897–7900.
(36) Maeda, F.; Hatsusaka, K.; Ohta, K.; Kimura, M. *J. Mater. Chem.* **2003**, *13*, 243–251.
(37) Ishikawa, N.; Sugita, M.; Ishikawa, T.; Koshihara, S.-Y.; Kaizu, Y. *J. Am. Chem. Soc.* **2003**, *125*, 8694–8695.
(38) Capobianchi, A.; Paoletti, A.M.; Pennesi, G.; Rossi, G.; Scavia, G. *Surf. Sci.* **2003**, *536*, 88–96.
(39) Vitali, L.; Fabris, S.; Conte, A.M.; Brink, S.; Ruben, M.; Baroni, S.; Kern, K. *Nano Lett.* **2008**, *8*, 3364–3368.
(40) Liu, Y.-Q.; Zhu, D.-B.; Ruan, L.-K.; Bai, C.-L.; Yamada, A.; Shigehara, K. *Chin. J. Chem.* **1991**, *9*, 126–130.
(41) Jones, R.; Krier, A.; Davidson, K. *Thin Solid Films* **1997**, *298*, 228–236.
(42) Miyake, K.; Hori, Y.; Ikeda, T.; Asakawa, M.; Shimizu, T.; Sasaki, S. *Langmuir* **2008**, *24*, 4708–4714.
(43) Gómez-Segura, J.; Díez-Pérez, I.; Ishikawa, N.; Nakano, M.; Veciana, J.; Ruiz-Molina, D. *Chem. Commun.* **2006**, 2866–2868.
(44) Miyake, K.; Fukuta, M.; Asakawa, M.; Hori, Y.; Ikeda, T.; Shimizu, T. *J. Am. Chem. Soc.* **2009**, *131*, 17808–17813.
(45) Takami, T.; Arnold, D.P.; Fuchs, A.V.; Will, G.D.; Goh, R.; Waclawik, E.R.; Bell, J.M.; Weiss, P.S.; Sugiura, K.; Liu, W.; Jiang, J. *J. Phys. Chem. B* **2006**, *110*, 1661–1664.
(46) Yang, Z.-Y.; Gan, L.-H.; Lei, S.-B.; Wan, L.-J.; Wang, C.; Jian, J.-Z. *J. Phys. Chem. B* **2005**, *109*, 19859–19865.
(47) Ye, T.; Takami, T.; Wang, R.; Jiang, J.; Weiss, P.S. *J. Am. Chem. Soc.* **2006**, *128*, 10984–10985.
(48) Klymchenko, A.S.; Sleven, J.; Binnemans, K.; De Feyter, S. *Langmuir* **2006**, *22*, 723–728.
(49) Binnemans, K.; Sleven, J.; De Feyter, S.; De Schryver, F.C.; Donnio, B.; Guillon, D. *Chem. Mater.* **2003**, *15*, 3930–3938.
(50) Takami, T.; Ye, T.; Arnold, D.P.; Sugiura, K.; Wang, R.; Jiang, J.; Weiss, P.S. *J. Phys. Chem. C* **2007**, *111*, 2077–2080.
(51) Otsuki, J.; Kawaguchi, S.; Yamakawa, T.; Asakawa, M.; Miyake, K. *Langmuir* **2006**, *22*, 5708–5715.
(52) Ma, H.; Yang, L.-Y.O.; Pan, N.; Yau, S.-L.; Jiang, J.; Itaya, K. *Langmuir* **2006**, *22*, 2105–2111.
(53) Zhang, Y.F.; Isshiki, H.; Katoh, K.; Yoshida, Y.; Yamashita, M.; Miyasaka, H.; Breedlove, B.K.; Kajiwara, T.; Takaishi, S.; Komeda, T. *J. Phys. Chem. C* **2009**, *113*, 9826–9830.
(54) Tanaka, H.; Ikeda, T.; Yamashita, K.; Takeuchi, M.; Shinkai, S.; Kawai, T. *Langmuir* **2010**, *26*, 210–214.
(55) Tanaka, H.; Kawai, T. *J. Vac. Sci. Technol. B* **1997**, *15*, 602–604.
(56) Tanaka, H.; Hamai, C.; Kanno, T.; Kawai, T. *Surf. Sci.* **1999**, *432*, L611–L616.
(57) Sugiura, K.-I.; Tanaka, H.; Matsumoto, T.; Kawai, T.; Sakata, Y. *Chem. Lett.* **1999**, 1193–1194.
(58) Katoh, K.; Yoshida, Y.; Yamashita, M.; Miyasaka, H.; Breedlove, B.K.; Kajiwara, T.; Takaishi, S.; Ishikawa, N.; Isshiki, H.; Zhang, Y.F.; Komeda, T.; Yamagishi, M.; Takeya, J. *J. Am. Chem. Soc.* **2009**, *131*, 9967–9976.
(59) Lei, S.-B.; Deng, K.; Yang, Y.-L.; Zeng, Q.-D.; Wang, C.; Jiang, J.-Z. *Nano Lett.* **2008**, *8*, 1836–1843.
(60) Kong, X.; Lei, S.; Yang, Y.; Deng, K.; Qi, G.; Wang, C. *Nano Res.* **2009**, *2*, 235–241.
(61) Yoshimoto, S.; Sawaguchi, T.; Su, W.; Jiang, J.; Kobayashi, N. *Angew. Chem. Int. Ed.* **2007**, *46*, 1071–1074.
(62) Otsuki, J.; Komatsu, Y.; Kobayashi, D.; Asakawa, M.; Miyake, K. *J. Am. Chem. Soc.* **2010**, *132*, 6870–6871.